Investigation of the Compositional Effect of Mixed Gas of Heavy and Light Gas Species on the Parameters of Mixed Plasma Driven by Pulsed Power Discharge

L. Malith M. De SILVA[1)]*, Taichi TAKEZAKI[2)],
Kazumasa TAKAHASHI[1)], Takashi KIKUCHI[1)], Toru SASAKI[1)]

[1)] *Nagaoka University of Technology, Nagaoka, Niigata 940-2137, Japan*
[2)] *University of Toyama, Gofuku, Toyama 930-8555, Japan*

(Received 4 October 2024 / Accepted 22 April 2025)

A pulsed power discharge experiment was conducted to investigate the compositional effect on plasma parameters of a mixed gas plasma of argon (Ar) and helium (He) gases as the heavy and light species, respectively. As the plasma parameters, electron temperature, drift velocity, and ion density were estimated for different compositions of Ar and He. Electron temperature and drift velocity were estimated by line-pair and time-of-flight methods, respectively. Ion density was estimated by Faraday cup method. Line-pair method results obtained by Ar lines and He lines at each composition show that Ar and He are in different partial local thermal equilibrium (PLTE) states in the mixed gas. Different relaxation times between different atomic species confirm the deviation of LTE. Similar drift velocity estimated by Ar and He lines separately at each composition shows that the plasma is a homogenous mixture. Drift velocity decreases as the increment of the Ar percentage in the mixture since the average mass of the mixture increases.

Keywords: pulsed power discharge, solar wind, mixed gas plasma, partial local thermal equilibrium, relaxation time of elastic collisions

DOI: 10.1585/pfr.20.1406032

1. Introduction

The formation of cosmic rays (CRs) is an interesting astrophysical phenomenon that has not been completely understood. Fermi has explained CRs are produced at shock structures which are generated as a consequence of the interaction of fast space plasma flow with space magnetic fields [1]. Since the energy distribution of CRs is non-Maxwellian, they are considered as non-thermally formed high energy particles. Moreover, since the energy distribution of CRs follows the power-law-spectrum, the formation mechanism for the relativistic region has been theoretically well explained by the diffusive shock acceleration model [2–4]. However, the CR formation mechanism in the non-relativistic region is still unclear [5, 6].

Some laboratory-scale experiments [7, 8] and numerical simulations [9, 10] suggest that ions in a fast plasma flow can be accelerated when they interact with a perpendicular magnetic field. The proposed mechanism is that ions are accelerated by the induced electric field resulting from the compression of the magnetic field by the fast plasma flow. For this to occur effectively, the magnetic field must be sufficiently deformed by the plasma flow [7, 8]. The effectiveness of this process is evaluated by factors such as the Magnetic Reynolds number [7, 8] and the pressure balance between the plasma and the magnetic field [8]. Since these factors are directly associated with plasma parameters, investigating the plasma parameters is crucial for evaluating this ion acceleration process.

In space, CRs are formed when space plasma flows, such as solar winds, interact with the interstellar magnetic field. Solar winds are fast plasma flows consisting of a mixed gas generated by the expansion of solar flares, with typical velocities ranging from 200 to 900 km/s [11]. In addition to solar winds, most astrophysical objects, such as stars, nebulae, and black holes, are composed of mixed gas plasmas. Therefore, studying the behavior and parameters of mixed gas plasma is essential for modeling such astrophysical events in the laboratory context. Thus, in this experiment, we aim to investigate how plasma parameters vary in mixed gas plasmas of heavy and light gas species with different compositions in the pulsed-power discharge. A numerical simulation study related to mixed gas plasma [10] showed that light ions are further accelerated in the presence of heavy ions during the ion acceleration process. This suggests that the behavior of mixed gas plasma and the associated plasma parameters differ from those of pure gas plasma. Thus, most astrophysical phenomena are associated with mixed gas plasma,

Corresponding author's e-mail: malithpst@gmail.com

the compositional effect must be considered as an essential factor when evaluating or modeling related mechanisms.

In the recent past, various laboratory-scale experiments have been performed related to fast plasma flows. In those experiments, to produce fast plasma flows, high-power lasers or pulsed power discharge techniques are used [8, 12–19]. In this experiment, we used the pulsed power discharge technique, as it is easier to control the gas species and their ratios in the mixed gas plasma generated in this experiment compared to the laser technique. However, since the energy density of the plasma produced by gas discharge using pulsed power is comparatively low, the tapered cone plasma focus device (TCPFD) is used to increase the energy density of the produced plasma flow. To convert the produced multi-dimensional plasma flow by the TCPFD into one-dimensional plasma flow, a plasma guiding tube is mounted at the open end of the TCPFD [7, 8, 19, 20]. The plasma flow propagates through the guiding tube is used to estimate the plasma parameters.

In this study, fast plasma flow of heavy and light gas species and their mixtures have been produced by the pulsed power method with the TCPFD [8, 20, 21]. As the heavy and light species, argon (Ar) and helium (He) gases have been used respectively. To investigate the compositional effect on plasma parameters, the effect of each pure gas species and three various compositions of mixed gas have been considered. For instance, the portions of Ar percentage in the considered compositions of the mixed gas were 100% (pure Ar), 75%, 50% 25%, and 0% (pure He). Plasma parameters such as electron temperature, drift velocity, and ion density were estimated for various gas compositions. Temperature and drift velocity are estimated by a self-emission method and ion density is estimated by the Faraday cup method.

2. Experimental Setup

The schematic diagram of the experimental setup is shown in Fig. 1. The fast plasma flows were generated by the pulsed power discharge method with the tapered cone plasma focus device (TCPFD). TCPFD consists of an inner cone electrode and outer taper electrode. When the discharge begins, plasma is generated at the bottom of the TCPFD, forming a radial current sheet between the cone and taper electrodes. Due to the current flowing in the central axis, an associated circular magnetic field is induced, perpendicular to the current sheet as shown in Fig. 1. The Lorentz force exerted on the sheet as a result of the magnetic field causes the sheet to be accelerated toward the tip of the TCPFD. At the tip, plasma associated with the sheet is pinched to form a high-energy-density plasma. When plasma was ejected from the TCPFD as fast plasma flow, to form a one-dimensional fast plasma flow, a polyoxymethylene tube having 30 mm length was mounted at the open end of the TCPFD as shown in Fig. 1.

The discharge experiments were performed for various compositions of He and Ar gases at the control pressure of 0.5 Pa to generate the mixed gas fast plasma flows. For the compositional variation in the mixed gas plasma, the molecular ratio of Ar and He (n_{Ar}/n_{He}) was changed by controlling the flow rate of gases keeping the pressure at 0.5 Pa. Since the volume and temperature in the chamber are constant at a particular composition, the molecular ratio of Ar to He can be expressed in terms of partial pressure (P) as follows:

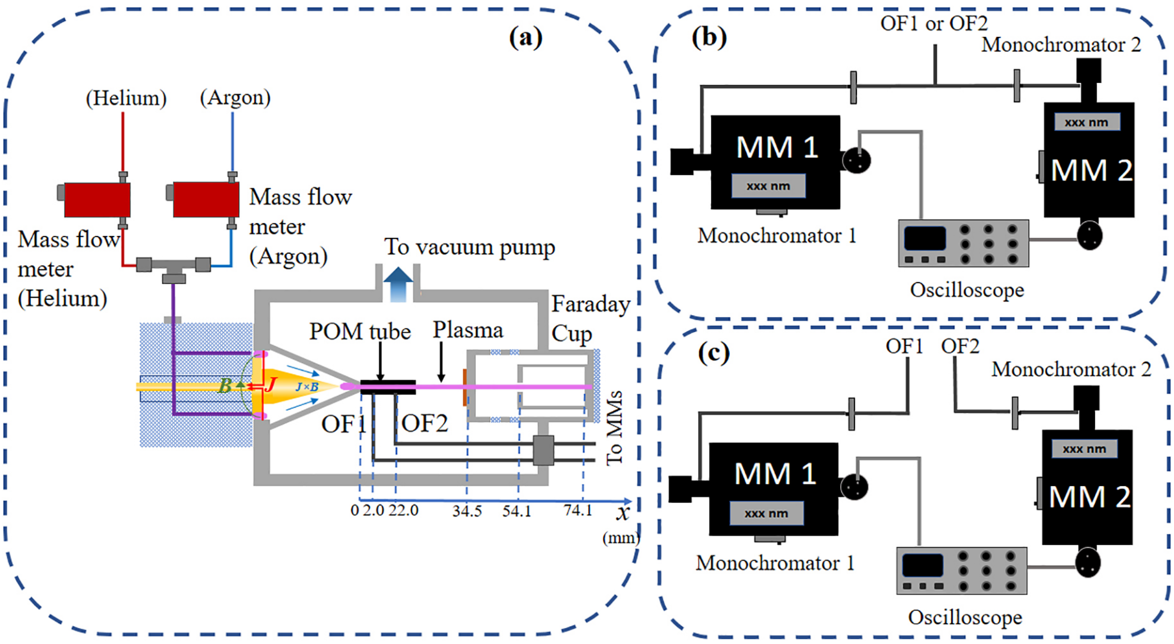

Fig. 1. (a) Schematic of the mixed gas experimental set up with the scale of the observation system. (b) Configuration of optical fibers, two monochromators, and oscilloscope in the electron temperature estimation, where both monochromators were connected to only one position (OF1 or OF2) at a time (c). Configuration of optical fibers, two monochromators and oscilloscope in the drift velocity estimation, where two monochromators were connected to OF1 and OF2 separately.

$$n_{\rm Ar}/n_{\rm He} = P_{\rm Ar}/P_{\rm He}\,. \tag{1}$$

To maintain the above relation at each composition, the required mass flow rates were estimated experimentally with the mass flow rate of standard cubic centimeter per minute (SCCM). To maintain the Ar portion of 100%, 75%, 50%, and 25% in the mixture, the estimated mass flow rates were 1.0, 0.45, 0.34, and 0.2 SCCM, respectively. Similarly, to maintain the He portion of 100%, 75%, 50%, and 25% in the mixture, the estimated mass flow rates were 5.1, 4.8, 4.0, and 2.0 SCCM, respectively.

For each composition, the electron temperature, drift velocity, and ion current were measured to investigate the compositional effect. Ion current waveforms were recorded by a Faraday cup. Self-emission of the plasma flow was recorded to estimate the electron temperature and drift velocity by the line-pair method and time-of-flight, respectively. An optical fiber system with two monochromators (BUNKOUKEIKI: M25-J750) was used with two different configurations to estimate the electron temperature and drift velocity as shown in Figs. 1(b) and (c), respectively.

The electron temperature was estimated at two positions on the propagating path of the plasma flow; optical fiber 1 (OF1) and optical fiber 2 (OF2), as shown in Fig. 1(a). At each position, the electron temperature was estimated for each composition with both Ar and He emission spectral lines by the line-pair method as a simplified version of the Boltzmann plot method [8, 22]. Two Ar-I spectral lines (415.9 and 696.5 nm) and two He-I spectral lines (402.6 and 706.5 nm) were used to estimate the electron temperature at both OF1 and OF2. The intensity ratio of selected emission lines was used to calculate the electron temperature as shown in Fig. 2(a). The time evolution of electron temperature at OF1 and OF2 was estimated by Ar-I and He-I lines. Moreover, the electron temperature variation as a function of the composition in the mixture also was estimated at both OF1 and OF2 by Ar-I and He-I lines.

The plasma drift velocity was estimated for each composition by time-of-flight method using both Ar and He emission lines. For that, Ar-II emission line (488.0 nm) and He-I emission line (447.1 nm) were used as in our previous study [8] since their intensities are comparatively stronger. Here, we estimated the velocity of the plasma front. Therefore, the time taken for the plasma front to travel between OF1 and OF2 is estimated by monochromator signals. When the plasma front reaches each OF, detection is started as the increment of the voltage on monochromator signals. Thus, considering the time points corresponding to voltage increment starting points on monochromator signals as shown in Fig. 2(b), the time-of-flight (T) was estimated. Since the physical distance between OF1 and OF2 is known (20 mm), the drift velocity of the plasma was estimated. Then the variation of the drift velocity as a function of the composition of the mixture was estimated.

3. Results and Discussion

3.1 Compositional effect on plasma drift velocity

Figure 3 shows the results of the compositional effect on the plasma drift velocity. Figures 3(a) and (b) show the signals of monochromators for velocity estimation by Ar line and He line, respectively. According to Figs. 3(a) and (b), it can be observed that the arrival time of the front of the plasma to the OF1 increases as the Ar percentage is increased in the mixture. Figure 3(c) shows the variation in drift velocity, experimentally estimated from both Ar line and He line, as well as the theoretical estimation from Eq. (2), as a function of the Ar and He percentages in the mixture. The velocity at each composition is the average of the velocities from three trials, and the associated error is the standard deviation of these three trials. According to Fig. 3(c), it can be observed that the drift velocity estimated by both Ar and He lines are the same in the considered three compositions of the mixed gas. It states that the plasma is a homogenous mixture, or otherwise, He and Ar species move together in the mixtures. In addition to that, drift velocity decreases as the Ar percentage is increased in the mixture as shown in Fig. 3(c). The reason is an increment of the time-of-flight as the increment of the average mass of the plasma as the increment of the Ar percentage in the plasma. Moreover, these results show that there is a compatibility between the increment of the arrival time of the plasma front to OF1 and the decrement of the drift velocity as the increment of the Ar percentage in the mixture following the inverse relationship between time and velocity.

When the energy input of the pure gas and the gas mixture is equal, the velocity ratio can be written as follows,

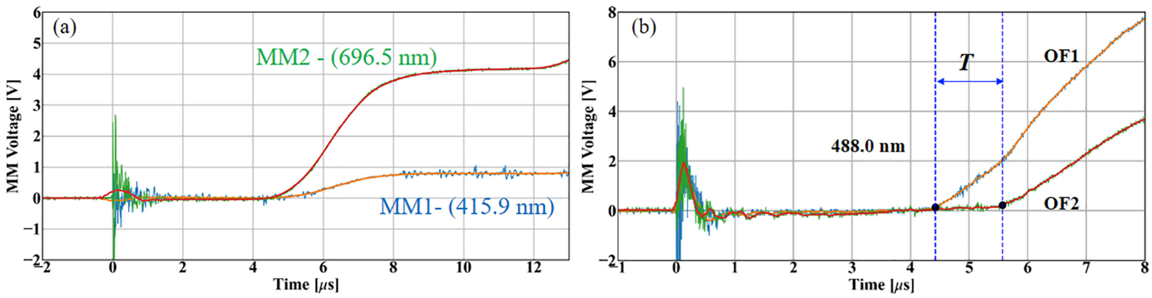

Fig. 2. Typical waveforms recorded by monochromators. (a) To estimate electron temperature in Ar 100% (only Ar) case. (b) To estimate the drift velocity in Ar 100% (only Ar) case.

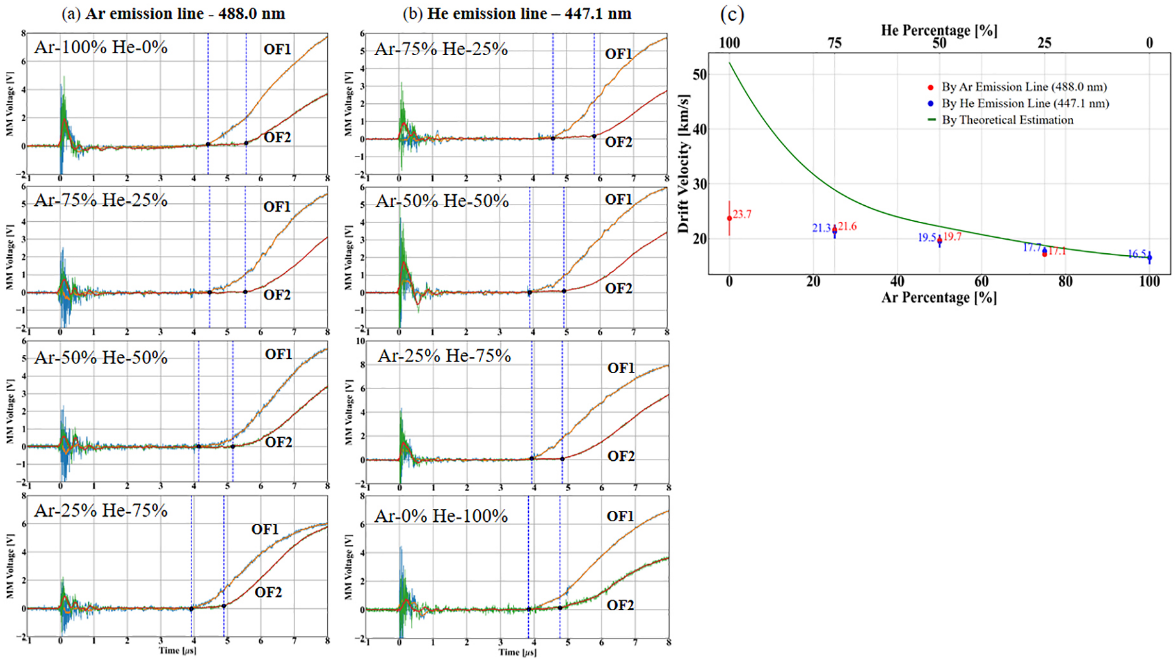

Fig. 3. Monochromators results for the estimation of the drift velocity by time-of-flight. (a) Comparison of monochromators results for the drift velocity estimation by Ar line at all the considered compositions. (b) Comparison of monochromators results for the drift velocity estimation by He line at all the considered compositions. (c) Comparison of drift velocities estimated by Ar emission line, He emission line, and theoretically as a function of Ar percentage in the mixture. Each velocity point is an average velocity of three trials and associated error is the standard deviation these three trials.

$$\frac{\upsilon_{\mathrm{mix}}^2}{\upsilon_{\mathrm{Ar}}^2} = \frac{1}{\eta_{\mathrm{Ar}} + (1-\eta_{\mathrm{Ar}})\frac{m_{\mathrm{He}}}{m_{\mathrm{Ar}}}}, \tag{2}$$

where, υ_{mix} is the velocity of mixture plasma, υ_{Ar} is the velocity of pure Ar gas discharge, η_{Ar} is the composition rate of Ar, m_{He} is the He mass, and m_{Ar} is the Ar mass. If the velocity of the Ar gas is considered as a reference, it is inversely proportional to the composition rate of Ar. While the theoretically estimated velocities tend to approximately agree with the experimentally estimated velocities up to about 50% of Ar composition in the mixture, the discrepancy becomes larger at lower Ar compositions. It indicates that the drift velocity of the mixed gas plasma is not determined solely by the mass ratio of compositional species. This discrepancy may be caused by the conversion process from the pulsed-power supply to the kinetic energy of the plasma, depending on the species, and this will be investigated in our future works.

3.2 Compositional effect on ion current waveforms

Figure 4 shows the ion current waveforms recorded by the Faraday cup for all the considered compositions. According to the results, it can be observed that the peak time of the bulk ion current increases as the Ar percentage is increased in the mixture. The reason to increase the peak time is the increment of the time-of-flight as the average mass of the plasma increases as the Ar percentage is increased in the mixture. This correlation between the peak time and the Ar percentage in the mixture agrees with the correlation between the plasma front arrival time to the OF1 and the Ar percentage in the mixture. This compatibility between ion current waveform results and monochromator results shows the compatibility between the self-emission measurements and Faraday cup measurements.

The ion number density n_i was calculated using the ion current waveforms measured by the Faraday cup as follows,

$$n_i = \frac{I_{\mathrm{peak}}}{T_{\mathrm{mesh}} ZeUS}, \tag{3}$$

where I_{peak} is the peak current of the ion current waveform, S is the cross-section of the aperture of the Faraday cup, U is the drift velocity of the plasma flow, e is the elementary charge, Z is the degree of ionization, and T_{mesh} is the transparency of the aperture mesh (65%). The velocity U is obtained by the time-of-flight method, and the current peak I_{peak} is obtained by the ion current waveform. Thus, the estimated ion number density indicates the maximum density of the plasma flow. We assume that the ion state is single-ionized ($Z = 1$).

Moreover, based on I_{peak} values in Fig. 4 and the estimated U values in Fig. 3(c), peak values of the ion densities were estimated as a function of the Ar percentage in the mixture as shown in Fig. 5. The associated error was estimated by applying the error propagation theory to Eq. (3) considering the experimental errors of I_{peak} and U. According to the results, the ion number density increases as the Ar percentage in the mixture is increased. The ionization energy of Ar (15.7 eV) is comparatively lower than that of the ionization energy of He (24.6 eV). Therefore, the possibility of generation of ions by Ar is higher than He. However, the ion number density remains on the order of 10^{21} m^{-3} even when the Ar fraction is changed. It indicates that the plasma produced by the pulsed

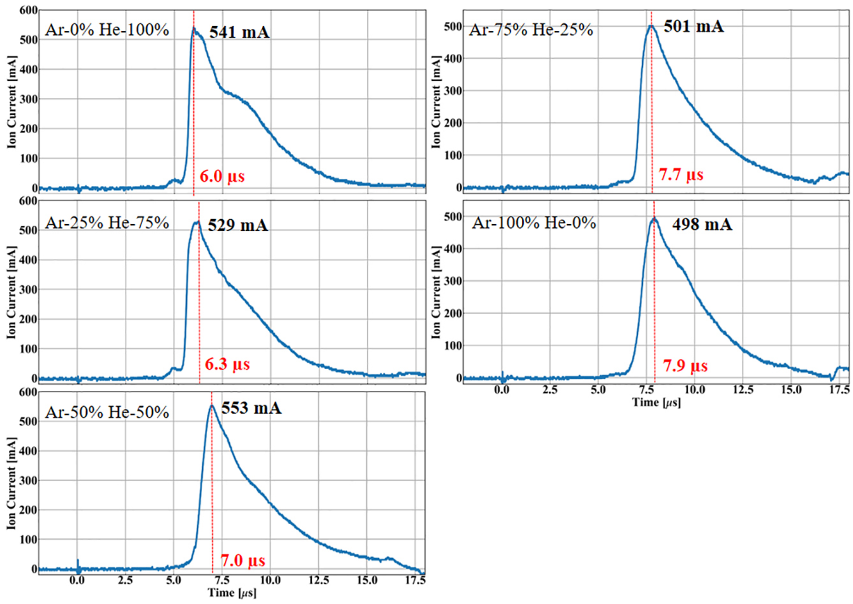

Fig. 4. Comparison of the compositional effect of mixed gas of Ar and He on the arrival time of the bulk ion current to the Faraday.

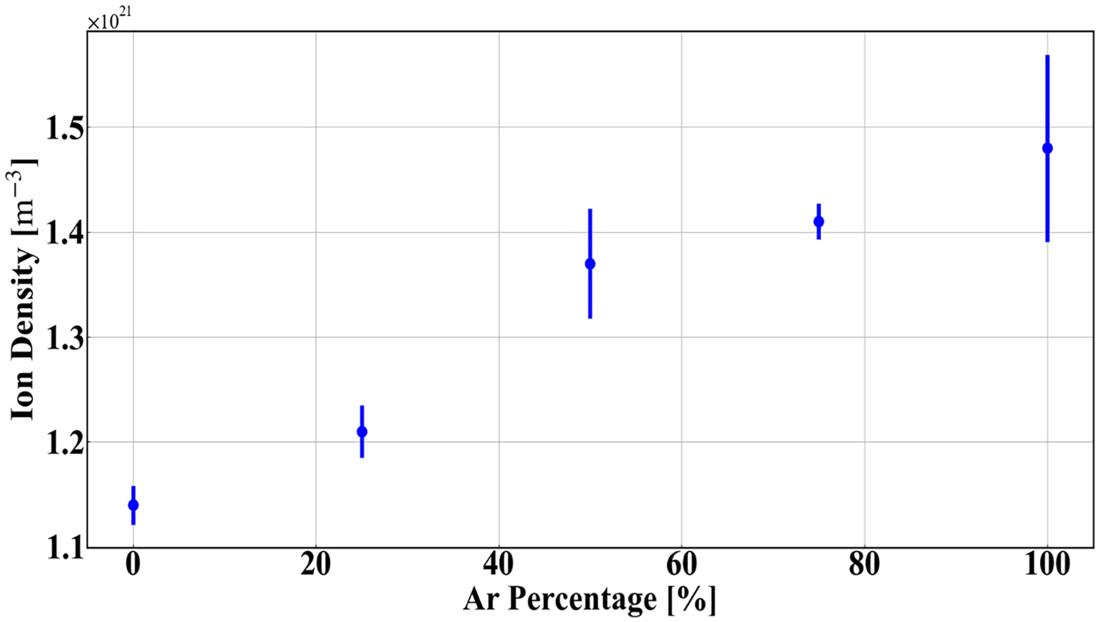

Fig. 5. Dependence of the ion number density on the Ar percentage. Value in each point was calculated using Eq. (3) and values in Figs. 3(c) and 4. Associated error was calculated using the uncertainties of peak current and velocity measurements.

power discharge is fully ionized even in the case of mixed gases. Moreover, ion density calculations show that the ion density (~ 10^{21} m^{-3}) is higher than the initial neutral particle density (~ 10^{20} m^{-3}), which is estimated using the ideal gas equation-of-state, considering the initial gas pressure to be 0.5 Pa. The higher ion density is due to the generated plasma being compressed by the pinching process, as explained in the working mechanism of the TCPFD in the experimental setup.

3.3 Compositional effect on electron temperature

Figures 6(a) and (b) show the time evolution of the electron temperature estimated in the plasma by Ar-I for all the considered compositions at both OF1 and OF2, respectively. Figure 6(c) shows the time evolution of electron temperature estimated in the plasma by He-I lines at OF2. The electron temperature at each time, in Figs. 6(a), (b), and (c), is the average of electron temperatures from three trials and the associated error is the standard deviation of these three trials. At OF1, the electron temperature estimated in the plasma by He-I lines became negative. In a previous research work performed by the same setup [8], the electron temperature estimated by both He-I lines and He-II lines by the same method at OF1 became negative. The reason for obtaining the negative electron temperature may be that the He has not reached the local thermal equilibrium (LTE) condition or even partial local thermal equilibrium (PLTE) condition at OF1 due to the

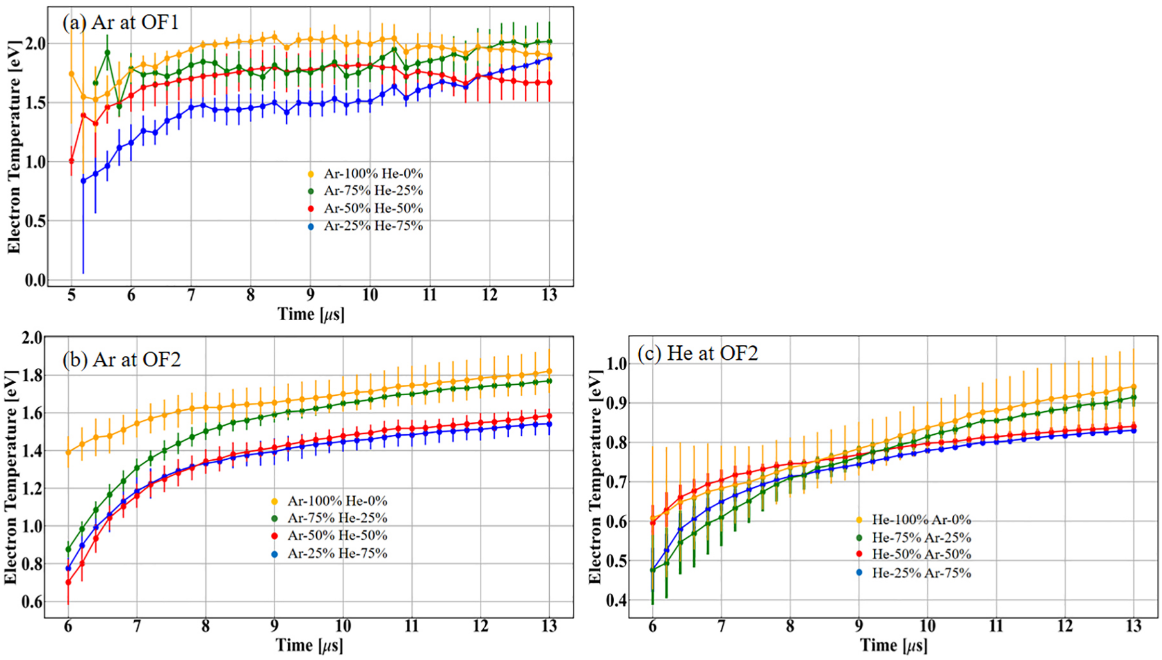

Fig. 6. Time evolution of electron temperature estimated by line-pair method in the mixed gas plasma for Ar and He. The electron temperature at each time point is the average of three trials and error bar represents the standard deviation of three trials. (a) Time evolution of electron temperature estimated by Ar-I lines at OF1 for all the considered compositions. (b) Time evolution of electron temperature estimated by Ar-I lines at OF2 for all the considered compositions. (c) Time evolution of electron temperature estimated by He-I lines at OF2 for all the considered compositions. The electron temperature at each time point is the average electron temperature of three trials and the associated error is the standard deviation of these three trials.

metastable states of He. Since OF1 is comparatively closer to the ejection of the electrode, a considerable amount of He atoms may be maintained in the metastable states. That results in a more populated metastable state than the ground state. Such a situation can cause an inverted population of energy levels. Due to the long lifetime of the metastable He [23], an inverted population of energy levels cannot be expected to be disturbed by rapid de-excitation. Thus, such an inverted population of energy level can lead to a negative electron temperature. However, the electron temperature estimation by He-I at OF2 was successful because He can reach the PLTE condition at OF2 since OF2 is located quite far away from the pinching point. Since the lifetime of metastable He is considerably longer, the de-excitation process by spontaneous emission is challenging to reach the PLTE at OF2. However, there is a possibility to be de-excited through a relaxation process such as collisional de-excitation [8]. Due to the experimental limitations of this experiment, this possibility cannot be precisely evaluated.

Figure 7 shows the electron temperature estimated by Ar-I lines and He-I lines as a function of Ar and He percentages in the mixture, respectively. The electron temperature estimated at each composition in Fig. 7 corresponds to the highest ion density region associated with the peak of the bulk ion current as shown in Fig. 4. Moreover, the electron temperature at each composition is the average electron temperature in the three trials. The associated error is the standard deviation of these three trials. According to the results for Ar in Fig. 7, the electron temperature increases with the Ar percentage at both OF1 and OF2. Moreover, these results are consistent with those in Figs. 6(a) and (b), as the time evolution of the electron temperature also increases with the Ar percentage. However, for He in Fig. 7, there is no clear correlation between the electron temperature and the He percentage at OF2. Similarly, although Fig. 6(c) shows that the electron temperature increases with time, there is no clear correlation with the He percentage during the first half of the time evolution (6–9 μs). Additionally, the electron temperature for He in Fig. 7 is related to the highest ion density point, which occurs in the first half of Fig. 6(c). Therefore, the electron temperature for He in Fig. 7 is consistent with the results in the first half of Fig. 6(c), in that the electron temperature is not correlated with the He percentage.

The electron temperature shown in both Figs. 6 and 7 corresponds to the Ar-I lines and He-I lines. Therefore, the estimated electron temperatures are associated with each species and represent the electron temperature relevant to those atomic species. However, the electron temperature estimated using line-pair method is associated with the free electrons. The electron temperatures derived from the Ar-I and He-I lines are indeed estimations of the electron temperature associated with free electrons, as the populations of the atomic excited states are determined by collisional excitation from the free electron population. These temperatures represent the thermal energy of free electrons in the plasma, which influences the atomic excitation and emission processes. Thus, assuming the PLTE condition, the excitation temperature estimated using atomic species is considered as the temperature

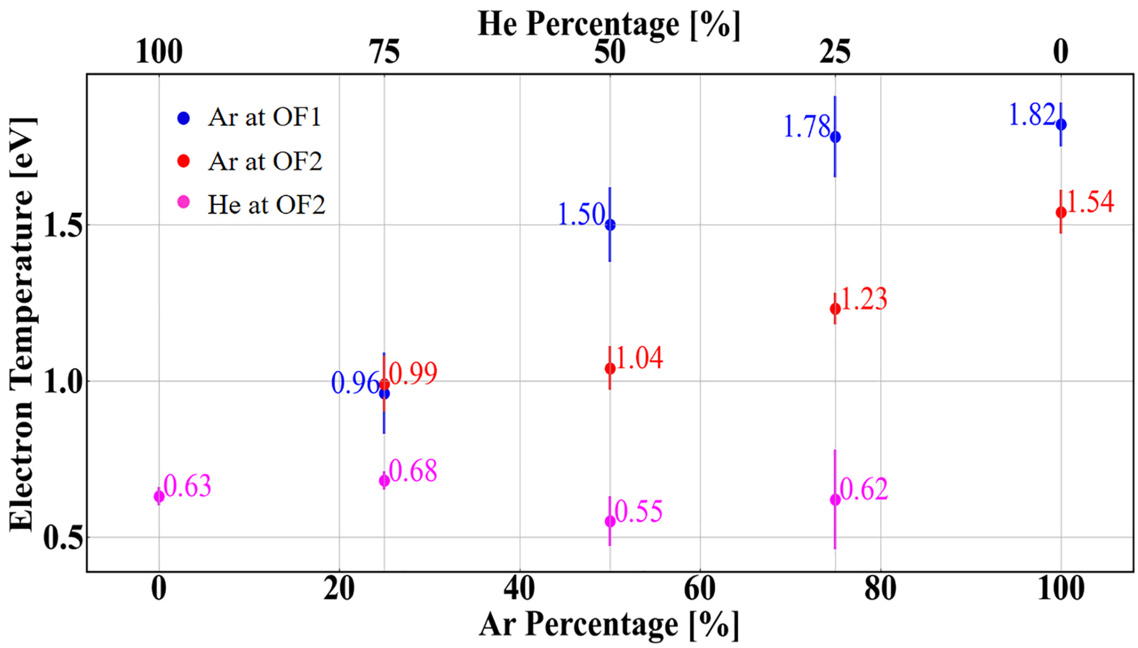

Fig. 7. Comparison of the electron temperature estimated by Ar-I emission lines and He-I emission lines.

of the associated free electrons for each species. Moreover, the results in both Figs. 6 and 7 clearly show that the electron temperature estimated in the plasma from the Ar-I lines and He-I lines differs for each composition. Therefore, it can be considered that there may be two distinct electron populations in the plasma. These two distinct electron populations in the plasma might be due to the different energy-transferring processes between electrons with Ar species and He species. Thus, these factors indicate that the system is not in the LTE state. However, since electron temperature using Ar-I lines and He-I lines is still possible despite the two distinct populations, achieving PLTE can be expected. A research work [24] reported that the electron temperature estimated by atomic species of hydrogen (H) and Ar by the Boltzmann plot method of a mixed gas plasma of H_2-Ar shows two different electron temperatures. Moreover, in that research work [24], it has been reported that the electron temperature estimated by atomic species of nitrogen (N) and Ar by the same method of a mixed gas plasma of N_2-Ar also shows two different electron temperatures. For these reasons, they have shown that the deviation of LTE conditions due to different relaxation times between different species [24]. Therefore, to evaluate the PLTE conditions of atomic species in this study also, the relaxation time (τ) of elastic collisions of neutral particles was estimated as follows [24]:

$$\tau_{(1-2)} = \frac{(m_1 + m_2)^2}{(2 m_1 m_2 v_1 N_2 \sigma_{12})}, \tag{4}$$

where $\tau_{(1-2)}$ is the relaxation time of species 1 when it collides with species 2, m_1 and m_2 are the atomic mass of species 1 and species 2, v_1 is the thermal velocity of species 1, N_2 is the number density of species 2, and σ_{12} is the cross section for collision between neutral atoms of species 1 and 2. This is a circular area in which the radius represents the sum of the radii of the colliding atoms. The relaxation time between two species can be used to explain the energy transferring between two species since there is an inverse relationship between the collisional frequency and the relaxation time. In this experiment, only atomic species of Ar and He were considered to calculate the relaxation times since Ar-I and He-I lines were used for electron temperature estimation.

Figure 8 shows the relaxation time of elastic collisions between the same species and different species as a function of the Ar percentage in the mixture. According to the results in Fig. 8, the relaxation times between different atomic species ($\tau_{(\text{Ar-He})}$ and $\tau_{(\text{He-Ar})}$) are larger than that of the relaxation times between the same atomic species ($\tau_{(\text{Ar-Ar})}$ and $\tau_{(\text{He-He})}$). It states that energy transfer between different atomic species is ineffective compared to between the same atomic species. Therefore, reaching a common temperature by all the species in the mixture is difficult. Thus, the mixed gas system cannot reach the common LTE and can only reach a PLTE condition in this pulsed power discharge experiment. The relaxation time between Ar atoms is shorter than He atoms at each composition. It states that the energy transfer by elastic collisions between Ar atoms is more effective than He atoms. That might be the reason for the electron temperature estimated by Ar lines is larger than the electron temperature estimated by He lines. Moreover, as shown in Fig. 8, the relaxation time of a particular atomic species decreases as the increment of the percentage of that gas species in the mixture. For instance, the relaxation time between Ar atoms decreases when the Ar gas percentage is increased in the mixture. It states that collisional frequency increases as a function of the percentage of that particular gas species in the mixture. That causes to increase the electron temperature estimated by a particular gas species as a function of the percentage of that particular gas species in the mixture.

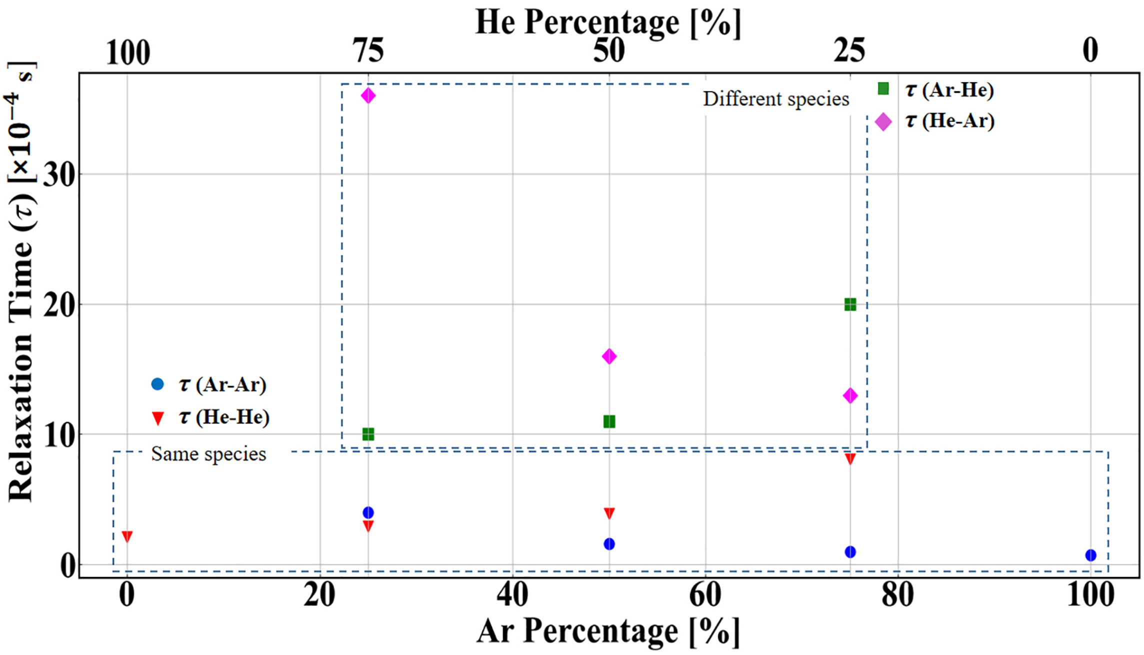

Fig. 8. Comparison of the relaxation time of collisions between same atomic species and different atomic species.

In addition, the collision in the plasma generated in this experiment was evaluated by comparing the drift time scale and the collisional time scales. The estimated parameters in this experiment pertain to the piston area (the main plasma bulk), where ions are dominant via the highly ionized state. Therefore, for the collisional times scale calculations, Coulomb collision time scales in ions were considered.

The drift time scale $\tau_D$was calculated as follows,

$$\tau_D = \frac{L}{\upsilon_D}, \tag{5}$$

where L is the system scale (22 mm) as shown in Fig. 1, and υ_D is the drift velocity.

The collisional time scale for collisions between ions of species 1 and 2 $\tau_{i(1-2)}$ was calculated as follows [25],

$$\tau_{i(1-2)} = \frac{16\pi\varepsilon_0^2 m_1 m_2 \upsilon_{i(1)}^3}{Z_1^2 Z_2^2 e^4 n_{i(2)} \ln \Lambda}, \tag{6}$$

where ε_0 is the permittivity of a vacuum, m_1 and m_2 are masses of ion species 1 and 2 respectively, $\upsilon_{i(1)}$ is the thermal velocity of ion species 1, Z_1 and Z_2 are the degree of ionization of species 1 and 2 respectively, $n_{i(2)}$ is the ion density of species 2. We assume that the ion state is single-ionized ($Z_1 = Z_2 = 1$). $\ln \Lambda$ is the Coulomb logarithm and that was calculated as follows [25],

$$\ln \Lambda = \ln\left(4\pi n_e \lambda_D^3\right), \tag{7}$$

where n_e is the electron density and it was assumed that $n_e = n_i$ since the generated plasma is highly ionized. λ_D is the Debye length.

The drift times and collisional times for ionic species are shown in Fig. 9. To assess the collisional nature of plasma, the ratio of $(\tau_{i(1-2)}/\tau_D)$ is considered. If the plasma is non-collisional, this ratio will be greater than 1. According to the calculations, $(\tau_{i(\mathrm{Ar}^+-\mathrm{Ar}^+)}/\tau_D)$ is in the order of 10^{-1}, while $(\tau_{i(\mathrm{He}^+-\mathrm{He}^+)}/\tau_D)$, $(\tau_{i(\mathrm{Ar}^+-\mathrm{He}^+)}/\tau_D)$ and $(\tau_{i(\mathrm{He}^+-\mathrm{Ar}^+)}/\tau_D)$, are in the order of 10^{-2}. Therefore, the $(\tau_{i(1-2)}/\tau_D)$ ratio is less than 1 for all the types of ion collisions. Thus, it can be stated that some collisions between ions occur in the plasma generated in this experiment.

4. Conclusion

We performed the experiment to investigate the compositional effect on plasma parameters of the mixed gas plasma of Ar and He generated by the pulsed power discharge. As the plasma parameters, the drift velocity, ion current density, and electron temperature were considered.

According to the plasma drift velocity results, it can be concluded that the mixed gas plasma generated in this experiment is a homogeneous mixture since drift velocities estimated by both Ar and He spectral lines separately at each composition are similar. Moreover, the drift velocity of the mixed gas plasma decreases as the Ar percentage is increased in the mixture due to the increment of the average mass of the gas mixture. This correlation is further confirmed by the decrement of the arrival time of the front of the plasma to OF1 as the Ar percentage is increased. The theoretically calculated and experimentally estimated drift velocities show approximate agreement up to 50% of Ar in the mixture. At lower Ar percentages, there is a discrepancy between calculated and experimental velocities. This may be caused by the conversion process from the pulsed-power supply to the plasma kinetic energy.

The ion number density increases in the mixed gas plasma as the Ar percentage is increased. However, the order of the magnitude is constant when the Ar percentage is changed. It

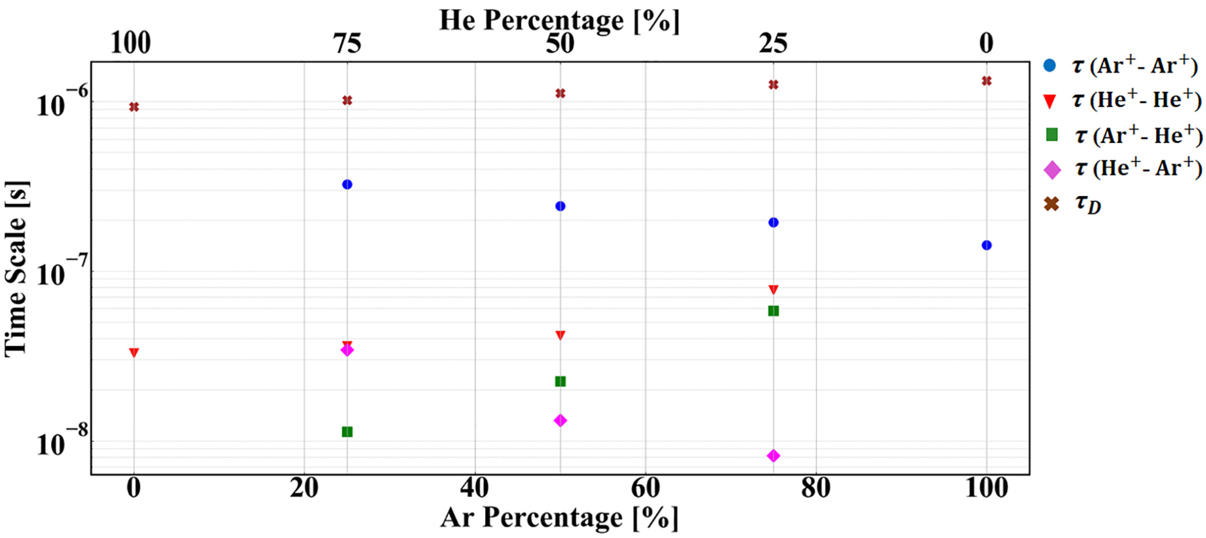

Fig. 9. Comparison of drift times and collisional times of collisions between ionic species.

states that the mixed plasma generated by this pulsed-power discharge experiment is highly ionized. Ion current waveforms show that there is a similar correlation between the arrival time of the front of the plasma to OF1 and the arrival time of the bulk ion current to the Faraday cup with the Ar percentage in the mixture. It shows the reliability of the self-emission measurement by the optical fiber system and the ion current measurements by the Faraday cup.

According to the electron temperature results, it can be concluded that Ar and He are in their own PLTE states due to two different electron temperatures estimated at each composition by Ar and He spectral lines. It has been further confirmed by the factor-of-10 difference of relaxation times between the same atomic species and different atomic species. Moreover, it can be concluded that electron temperature estimated by a particular gas species increases as a function of the percentage of that particular gas species in the mixture due to the increment of the collisional frequency. Moreover, smaller collisional time scales of Coulomb collisions between ionic species, compared to the drift time scale, reveal that the plasma is a collisional plasma.

In the future, we will conduct an experiment with the mixed plasma of Ar and He and a perpendicular magnetic field to investigate the compositional effect of mixed gas on the behavior of collisionless plasma in the non-relativistic domain.

Acknowledgment

This research work was partly supported by JSPS KAKENHI Grant No. 20K4440 and 23K13079.

[1] E. Fermi, Phys. Rev. **75**, 1169 (1949).
[2] S. Swordy, Space Sci. Rev. **99**, 85 (2001).
[3] A. Bell, Mon. Not. R. Astron. Soc. **182**, 147 (1978).
[4] K. Schure *et al.*, Space Sci. Rev. **173**, 491 (2012).
[5] R.A. Treumann, Astron. Astrophys. Rev. **17**, 409 (2009).
[6] Y. Ohira, Proceedings of the 7th International Workshop on Very High Energy Particle Astronomy in 2014 (VHEPA2014) 011002 (2017).
[7] T. Takezaki *et al.*, Phys. Plasmas **23**, 062904 (2016).
[8] L. M. M. De Silva *et al.*, Jpn. J. Appl. Phys. **63**, 09SP27 (2024).
[9] T. Takezaki *et al.*, High Energ. Dens. Phys. **33**, 100698 (2019).
[10] T. Takezaki *et al.*, Phys. Plasmas **28**, 102109 (2021).
[11] Y. Sun *et al.*, Space Weather **20**, p.e2022SW003128 (2022), https://doi.org/10.1029/2022SW003128
[12] C.M. Huntington *et al.*, Nat. Phys. **11**, 173 (2015).
[13] A. Casner *et al.*, High Energ. Dens. Phys. **17**, 2 (2015).
[14] Y. Kuramitsu *et al.*, High Energ. Dens. Phys. **17**, 198 (2015).
[15] Y. Sakawa *et al.*, High Energ. Dens. Phys. **23**, 207 (2017).
[16] N. Khasanah *et al.*, High Energ. Dens. Phys. **23**, 15 (2017).
[17] J.S. Ross *et al.*, Phys. Rev. Lett. **118**, 185003 (2017).
[18] T. Morita *et al.*, J. Phys. Conf. Ser. **244**, 042010 (2010).
[19] T. Oguchi *et al.*, Plasma Fusion Res. **18**, 2401049 (2023).
[20] T. Sasaki *et al.*, In Proceedings of the 12th Asia Pacific Physics Conference (APPC12) 015096 (2014).
[21] K. Kondo *et al.*, Rev. Sci. Instrum. **77**, 036104 (2006).
[22] G. Han and G. Cho, Appl. Sci. Converg. Technol. **26**, 201 (2017).
[23] S.S. Hodgman *et al.*, Phys. Rev. Lett. **103**, 053002 (2009).
[24] T. Kitamura *et al.*, ISIJ Int. **38**, 1165 (1998).
[25] W. Baumjohann and R.A. Treumann, *Basic Space Plasma Physics* (World Scientific Publishing Company, 2012).